Detection and Characterization of ZnO on a Passive Film of Pure Zinc

F. Touri[1], A. Sahari[1,], A. Zouaoui[1], F. Deflorian[2]*

[1]Laboratoire de Croissance et de Caractérisation de Nouveaux Semi-Conducteurs, Université de Sétif1, 19000, Algeria
[2] Department of Industrial Engineering, University of Trento, Via Mesiano 77, 38123 Trento, Italy
*E-mail: sahariali2000@yahoo.com

Zinc oxide (ZnO) thin films were grown by potentiodynamic polarization of a pure zinc surface in a chloride medium with different potential scan rates. It was found that the size of the ZnO films mainly dependedon the scan rate. Using oxygen as the precursor of the conversion reaction of the product formed during the scan potential, different morphologies of the films were obtained. The X-ray diffraction pattern and Raman spectraof the samples at different scan rates show the characteristic peaks of the ZnO wurtzite structure. At room temperature, photoluminescence tests showed a UV emission at approximately 390 nm , a visible emission at 442 and a deep-level emission in the green region at 523 nm, which are typical of ZnO.

1. INTRODUCTION

The anodic polarization of metals has been used for a long time to decorate metal surfaces and/or increase the corrosion resistance. This method is notably cost-effective to produce uniform oxide films and adhesives on metals [1]. Potentiodynamic polarization is a useful technique in corrosion studies. The method informs us more about the corrosion phenomena of metals, and the shape of the complete experimental curve (anodic and cathodic branches) may indicate the nature of the reaction at the corrosion potential, e.g., whether the metal is active, passive or active/passive in the corrosion environment [2]. Moreover, many works have been devoted to understanding the zinc oxidation mechanism, particularly the dissolution–passivation phenomenon at low potentials because of the technical importance of aqueous alkaline batteries made from this metal [3–5]. The resistance of

zinc to corrosion depends strongly on the compounds formed on the surface of the metal and also on the structure of these compounds [6–15]. The oxide layer on Zn in contact with aqueous electrolytes consists of an outer oxide/hydroxide film (known as Type-I Zn oxide) and an inner compact layer (known as Type-II Zn oxide) [16-21]. The inner layer has been postulated to form by the direct oxidation of Zn to ZnO, which is driven by a cathodic reaction such as oxygen reduction on the surface of the ZnO semiconductor [22-25]. Zn^{2+} ions may be ejected through the ZnO film and precipitate to Type-I Zn porous oxides [18,20,24]. One can change the outer precipitated layer by varying the composition of the environment and enhance the barrier properties of type-I oxides. The barrier properties are related to the thickness, compactness, porosity, electrical conductivity and surface charge of these oxides [9-11, 14, 25]. We are notably interested in the composition of the passive film formed during the anodic polarization of a zinc surface and more particularly in ZnO, which has interesting optical properties. Consequently, this study will focus on this element. In fact, our idea was inspired by a Pourbaix diagram, which suggests that ZnO may be present in the composition of the passive film formed by the anodic polarization of pure zinc in a slightly basic medium. This study only demonstrates the effect of some parameters of the anodic polarization method such as the scanning potential and pH. In this context, we report a simple linear polarization of pure zinc to synthesize ZnO. It consists of the anodic oxidation of pure metallic Zn in slightly alkaline media (8<pH<9) by scanning the potential from the open circuit (OPC) potential to anodic potentials, where zinc oxidation occurs. In this method, the passivation of pure zinc requires strong scanning rate control. Therefore, to study the ZnO growth using this method, the morphologies of ZnO films will be observed. The objective of this work was to determine the optimized scan rate to form a controlled nanostructure in the passivation region of the metal. Nanoflakes of ZnO films were prepared on a zinc substrate using linear voltammetry (LV) with no template, surfactant or seed layer. We also investigated the effect of oxygen as a precursor in the ZnO formation. The final ZnO films were characterized using cyclic voltammetry (CV), scanning electron microscopy (SEM), X-ray diffraction, Raman spectroscopy (RS) and photoluminescence (PL)

2. EXPERIMENTAL PROCEDURE

Square pieces of Zn (5x5 mm^2; purity 99.999%) were used as the starting material. The zinc foils were cleaned with acetone in an ultrasonic bath for 5 min, washed with ethanol and deionized water, and dried in a nitrogen steam. The electrolyte solution was sodium chloride (0.1 M NaCl). The pH was adjusted to 9 by adding sodium hydroxide. Anodic polarization experiments were performed with a Potentiostat/Galvanostat VoltaLab 40 at different scanning rates. A conventional three-electrode system was used. A platinum sheet was used as the auxiliary electrode, the working electrode was a pure zinc electrode, and the reference electrode was a saturated calomel electrode (SCE) with a Luggin capillary positioned near the working electrode surface to minimize the ohmic potential drop. After the oxidation of pure Zn by linear voltammetry, all samples were dried at 120 °C. A passive layer was observed on the surface of pure zinc. The surface morphology of the ZnO nanostructures were imaged by scanning electron microscopy(SEM) with a GEOL 7001F microscope coupled with energy

dispersive X-ray (EDX). The X-ray diffraction (XRD) analyses were performed on an INEL CPS120 diffractometer using filtered CuKα (λ = 0.15406 nm) as a radiation source. The diffractometer was operated at 40 kV and room temperature; the XRD analyses were performed for the scattering anglesof 25-90°. Raman spectroscopy was performed by Labram1b using 659.3-nm waves. The emission and excitation spectra were obtained using a Perkin-Elmer (LS-50B) luminescence spectrometer with pulsed Xe lamp excitation at room temperature.

3. RESULTS AND DISCUSSION

3.1. Potentiodynamic polarization measurements

Fig.1 shows different steps of the potentiodynamic oxidation of zinc. Zn was oxidized in 0.1 NaCl solution at pH = 8 with various scan rates of 1, 3, and 5 mV/s. The potentiodynamic sweep began at an open circuit potential (O.P.C. = -1020 mV). To remain in the metal passivation area, the potential scan was stopped at 2 V. For lower scan rates (1and 3 mV/s),the current increased at the beginning of the potential scan because of the Zn oxidation and passivation phenomena. The current was maximal at points a_1 and a_2 at -0.39 and -0.40 V for the low scan rates of 1 and 3 mV/s, respectively.
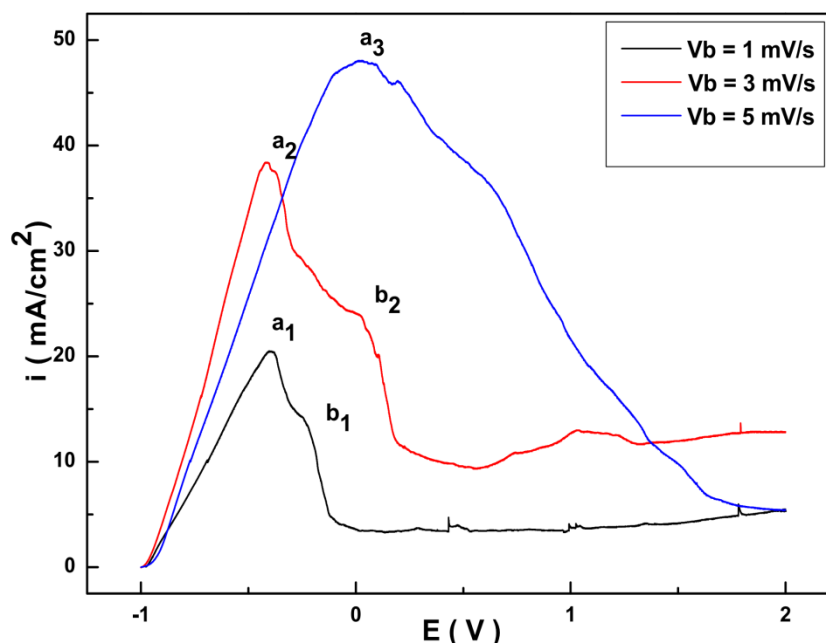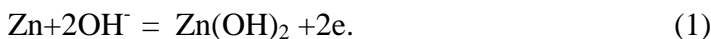

Figure 1. Polarization curves of pure Zn in 0.1Mol/L NaCl at various potential scan rates.

This first peak is associated with the formation of $Zn(OH)_2$. After this step, the current strongly decreased to points b_1 and b_2,where a second peak appeared, which corresponds to the formation of a less conductive film of ZnO. When the scan continued, the current became stable, which indicates a large zinc passivation area [26-27]. Most authors generally accept that the Zn passivation begins with
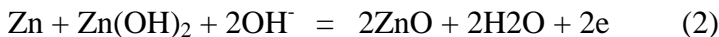
the precipitation of zincate ion $Zn(OH)_4^{2-}$ to $Zn(OH)_2$ and ZnO as the protective film. In summary, the outer precipitated layer comprises both precipitated ZnO and $Zn(OH)_2$.

The conceivable mechanisms of the formation of these films are as follows:

1-   Zn oxidation

$$Zn + 2OH^- = Zn(OH)_2 + 2e. \qquad\qquad (1)$$

2- $Zn(OH)_2$ oxidation

$$Zn + Zn(OH)_2 + 2OH^- = 2ZnO + 2H2O + 2e \qquad (2)$$

More details of the formation mechanisms of $(ZnOH)_2$ and ZnO are presented in references [27-31].With the 5-mV/s scan rate (blue line), the behavior is slightly different: the current increases and strongly decreases with only one peak at a_3. The second peak is not well formed. The zinc passivation area begins notably early for small scan rates (1 and 3 mV/s).If we associate the first and second peaks with the formations of $Zn(OH)_2$ and ZnO films, respectively, we can speculate that at scan rates of 5 mV/s (relatively highs scan rates), ZnO is not completely formed or the $Zn(OH)_2$ transformation is notably fast. In other words, it is difficult to distinguish between $Zn(OH)_2$ and ZnO formations at 5 mV/s based on the polarization curves.

3.2. Morphological study
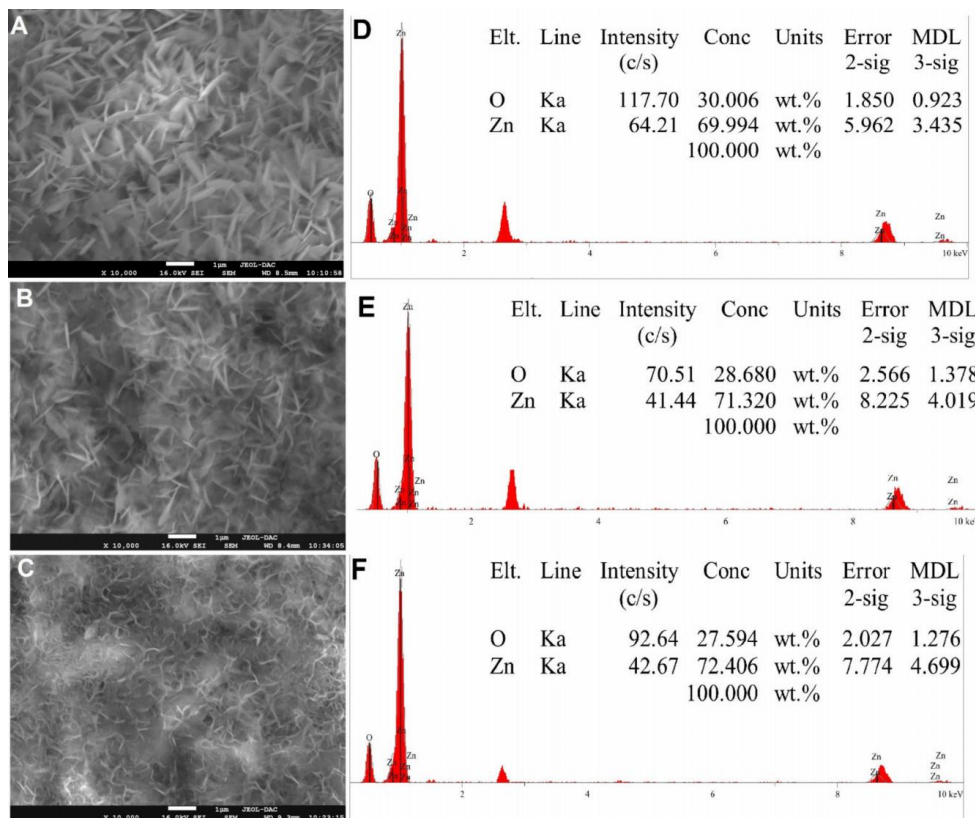
Figure 2. SEM images and EDX spectra of ZnO obtained by Potentiodynamic polarization of pure zinc at (A) 1mV/s, (B) 3mV/s, and(C) 5 mV/s.

The films prepared at room temperature with scan rates of 1, 3, and 5 mV/s were imaged using SEM. The corresponding images A, B and C are shown in Fig.2.These films are characterized by the presence of ZnO grains on the surface with edge-like structures. In addition, at 5 mV/s (Fig.2 C) the film exhibits less dense and smaller ZnO grains. By decreasing the scan rate, we changed the ZnO growth with large-sized grains (Fig.2 B), and the surface became increasingly occupied. At a lower scan rate (1 mV/s) the formed ZnO appeared denser and larger (Fig.2 A) because the ZnO formation had sufficient time to develop. According to these results, the film morphology is notably sensitive to the scanning rate of the anodic oxidation of pure zinc. The EDX figures (D, E and F) show the composition of the films at 1, 3 and 5 mV/s, respectively. At lower scan rates, the ZnO amount is large. According to these results, the zinc oxidation by linear sweep of potential forms ZnO, particularly if the experiment is conducted at low scanning rates. This behavior reminds us to consider further investigation at lower scan rates.

### 3.3. ZnO preparation at low scanning rates and with oxygen
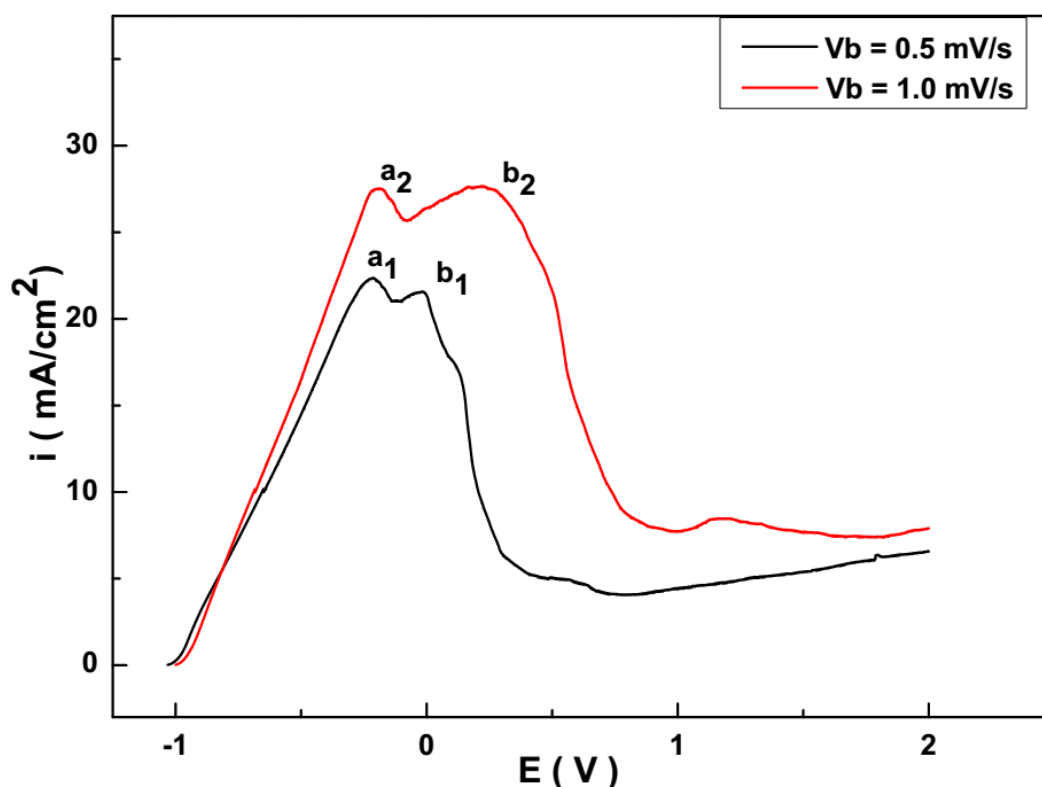
Figure 3. Polarization curves of pure zinc in the presence of oxygen in 0.1Mol/L NaCl at scan rates of 0.5 (black line) and 1 mV/s (red line).

Two low scanning rates (0.5 and 1.0 mV/s) were used to study the zinc oxidation in 0.1 Mol/lNaCl. This time, the study was conducted in the presence of bubbled oxygen through the solution for 20 min. The oxygen was used as a precursor to form ZnO. The electrochemical behavior of zinc electrodes is shown in Fig.3. This figure indicates the presence of two peaks in each curve: a_1 and a_2,

which are associated with zinc oxidation (reaction 1), and b_1 and b_2, which are associated with $Zn(OH)_2$ oxidation and the formation of ZnO (reaction 2).

The current density of peaks increases with increasing scan rate, and its potential slightly shifts towards positive values. These findings are confirmed in the literature [29, 32].
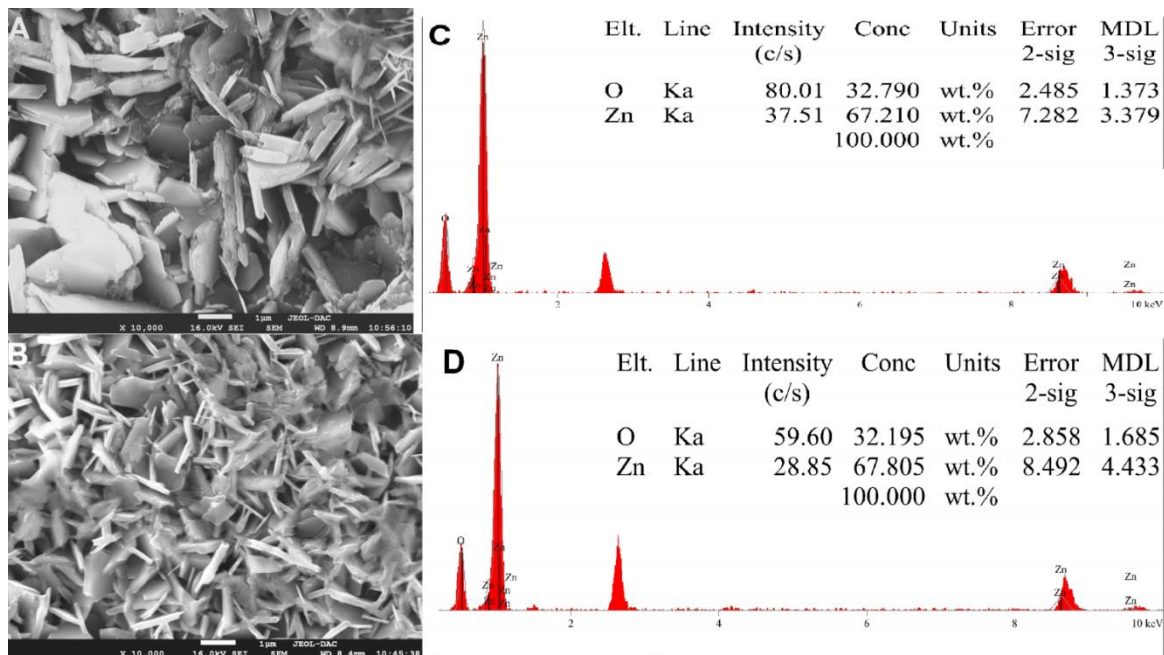

Figure 4. SEM images and EDX spectra of ZnO obtained by the potentiodynamic polarization of pure zinc at (A) 0.5 mV/s and (B) 1mV/s under bubbling oxygen for20 min in 0.1 Mol/L NaCl.

Figs. 4 A and B show the surface morphology after oxidation of the Zn surface in 0.1 Mol/L NaCl at 0.5 and 1.0 mV/s, respectively,while bubbling oxygen for 20 min. At low scan rates, the surface appears more occupied with notably dense and large ZnO grains (image A). In image B, where the oxidation occurred at 1.0 mV/s, the surface appeared more occupied by small ZnO grains. The presence of oxygen plays an important role in the oxidation process, strongly modifies the surface morphologies, and causes the ZnO formation. The driving corrosion reaction is:

$$\frac{1}{2}O_2 + H_2O + 2\grave{e} \leftrightarrow 2OH^-$$
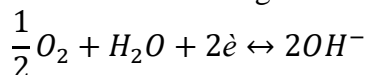
Zinc is oxidized to zinc ions via the application of an anodic potential as follows:

$$Zn \leftrightarrow Zn^{2+} + 2\grave{e}.$$
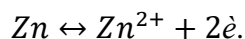
The oxidation of zinc begins when oxygen is reduced to hydroxide ions on the zinc surface, and a thin passive layer of oxide is formed. Several papers in the literature show that the interaction of zinc with sodium chloride in the presence of gaseous oxygen produces various compounds with zinc hydroxychloride precipitation and zinc oxides [33-34]. According to our results, the presence of a high amount of oxygen, the localized pH and the low scan rate are responsible for the formation of aligned zinc oxide on the electrode surface. C and D are the corresponding EDX spectra

of images A and B, respectively. The EDX indicates the presence of Zn and O with insignificant differences in composition. The EDX result for sample (d) confirms the presence of only oxygen and zinc, which indicates that a continuous and pure ZnO coating was formed.

3.4. Structural characterization of ZnO prepared at low scan rates under bubbling oxygen
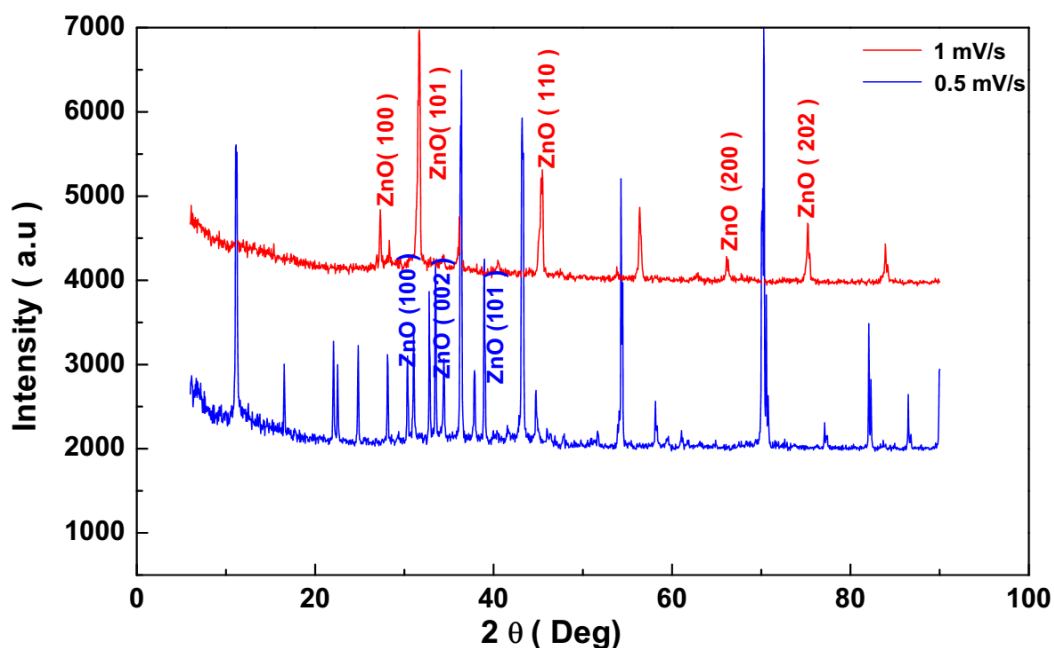
Figure 5. XRD patterns for ZnO at 0.5 and 1.0 mV/s under bubbling oxygen in0.1 Mol/L NaCl.

The XRD patterns of the passive layers formed at scan rates of 0.5 and 1.0 mV/s are shown in Fig.5. The two films exhibit hexagonal ZnO wurtzite structures with visible (101), (100), (110), (200),and (002) peaks. Thus, oxide particles have predominantly good crystallinity, and dominant diffraction peaks were assigned to the major crystalline product. Strong reflections that correspond to the (101) planes were observed for films that were produced at 1 mV/s with weaker reflections of (1 0 0) and (002) observed only for the film at 0.5 mV/s.

In the case of zinc passivation at 1.0 mV/s, the obtained film was strongly textured with the (100) preferential orientation and weaker reflections of the (101), (110), (200), and (202) planes of wurtzite ZnO [35], which is consistent with the common growth habits of ZnO films deposited using other methods[36-39].

3.6. Raman spectroscopy

Figs. 6 (a b, c) show the evolution of the Raman spectra as a function of the scan rate for ZnO nanorods, which were prepared at scan rates of 0.5, 1.0 and 1.5 mV/s, respectively. The frequencies of the fundamental optical mode in ZnO are E_2 (low) = 101 cm^{-1}, E_2 (high) = 437 cm^{-1}, A_1 (TO) = 380 cm^{-1}, A_1(LO) = 574 cm^{-1}, E_1(TO) = 407 cm^{-1}, and E_1 (LO) = 583 cm^{-1} [40]. For all spectra measured in

the range of 100-1600 cm^{-1}, the sample produced at 0.5 mV/s had two peaks at approximately 438cm^{-1} and 579.36 cm^{-1}, which are believed to be characteristic scattering peaks of the Raman-active dominant E$_2$ high mode of wurtzite hexagonal ZnO [41]. The intensity of the Raman peaks increases with decreasing scan rate because of the increasing volume of ZnO with a long duration of zinc passivation at low scan rates. The Raman spectrum of polished Zn is also shown in Fig.6, but no characteristic peaks are observed.
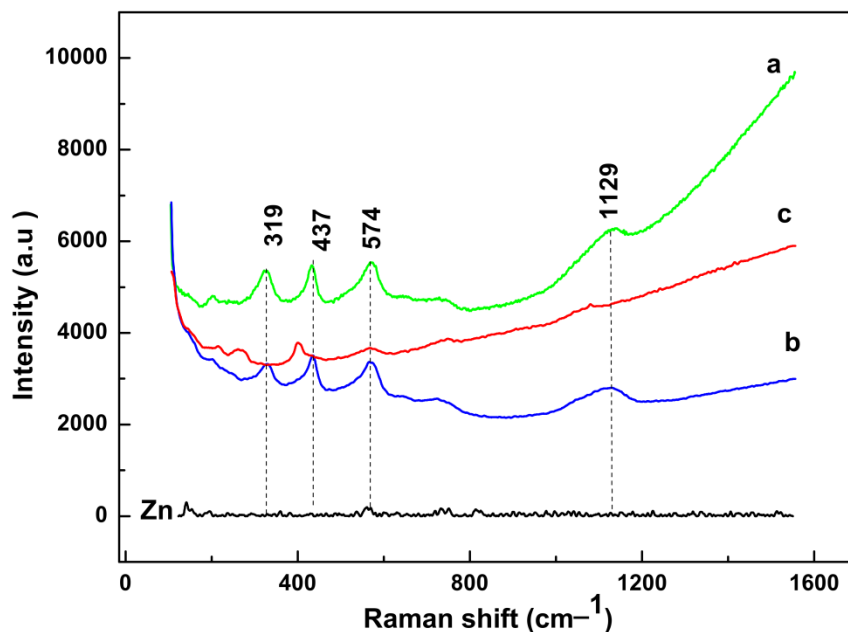

Figure 6. Raman spectra for passivated Zn at (a) 0.5, (b) 1 and (c) 1.5 mV/s. Characteristic peaks of ZnO are identified.

Fig. 7 shows the room-temperature PL spectra of ZnO prepared at -0.5 and -1.0 (low scan rates). In the presence of oxygen, both spectra show the UV emission at 390 nm (peaks a$_1$ and a$_2$ for -0.5 and -1.0 mV/s and the green deep-level (DL) emission peak at approximately 523 nm (c$_1$ and c$_2$ for -0.5 and -1.0, respectively).

The UV line (390 nm) corresponds to the band-edge emission and is attributed to the radiative recombination of excitons, whereas the green emission (523 nm) is assigned to the charge carrier relaxation through surface-related trap states [42-43]. The intermediate peaks b$_1$ and b$_2$at 442 nm can be attributed to the oxygen vacancies, interstitial Zn or transition between defects (interface traps) at the grain boundaries and the valence band [44, 45]. As observed, at low scan rates (0.5 and 1.0 mV/s), the intensities are more significant. However, the commonly observed broad DL emission in the green region is believed to reduce the intensity of the ultraviolet (UV) emission [46]. Therefore, enhancement of the UV emission and decrease in the green DL emission of ZnO nanostructures has become one of the important issues in the research of ZnO materials in recent years.
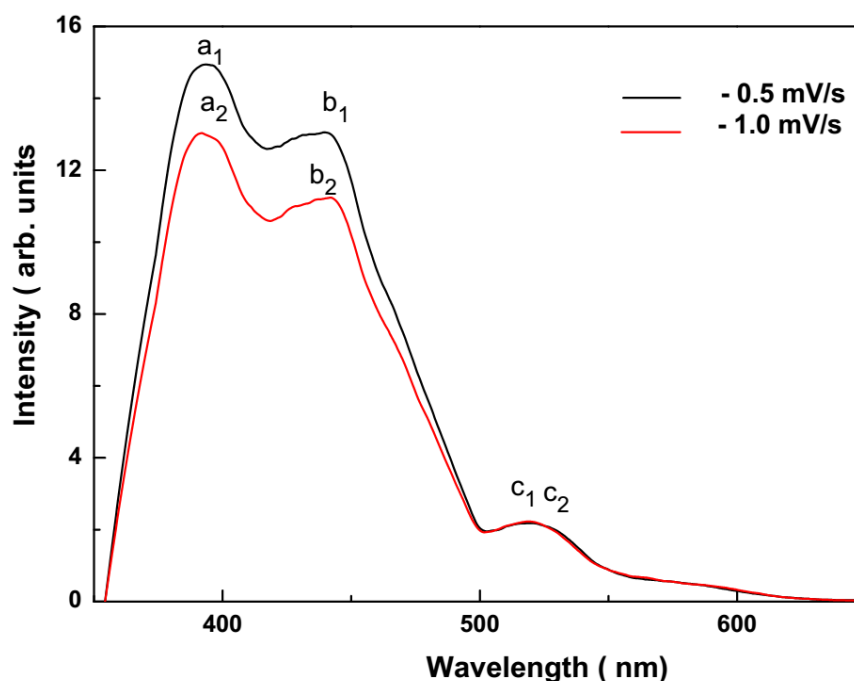
Figure 7. PL spectra of ZnO formed by the Potentiodynamic polarization of pure zinc with bubbling oxygen for 20 min in 0.1 Mol/L NaCl.

4. CONCLUSION

ZnO was prepared through controlled zinc passivation using the linear potentiodynamic method. The method is inexpensive and easy to implement. The scan rate is the main key to prepare ZnO. At low scan rates, zinc-passivated surfaces with dense grain size formed under oxygen bubbling. Without oxygen and with a relatively high scan rate, the surface is characterized by small grains scattered over the entire surface. The diffraction peaks of all samples can be well indexed to the hexagonal wurtzite structure of ZnO. Raman spectroscopy revealed a characteristic scattering peak of the Raman-active dominant E_2 high mode of wurtzite hexagonal ZnO. The PL spectra revealed the optical properties of ZnO nanostructures: a UV emission band centered at approximately 390 nm, a visible emission band in the range of 420-425 nm and a green emission centered at approximately 523 nm.

References

1. P.A. Malachesky, in: A.J. Bard (Ed.), *Encyclopedia of Electrochemistry of the Elements*, vol. VI, Marcel Dekker, New York and Basel, 1973, p. 63.
2. Harvey J. Flitt, D. Paul Schweinsberg, *Corros. Sci*. 52 (2010) 1905.

3. J. McBreen, Rechargeable, *J. Electroanal. Chem*. 168 (1–2) (1984) 415.

4. L. Baugh, A. Higginson, *Electrochim. Acta* 30 (1985) 1163.

5. L.M. Baugh, A.R. Baikie, *Electrochim. Acta* 30 (9) (1985) 1173.

6. I.S. Cole, T.H. Muster, D. Lau, N. Wright, N.S. Azmat, *J. Electrochem. Soc*.157 (2010) C213.

7. T.H. Muster, I.S. Cole, *Corros. Sci*. 46 (9) (2004) 2319.

8. R. Krieg, M. Rohwerder, S. Evers, B. Schuhmacher, J. Schauer-Pass , *Corros. Sci*. 65 (2012) 119.

9. I.S. Cole, T.H. Muster, S. Furman, N. Wright, A. Bradbury, J. *Electrochem. Soc*. 155 (2008) C244.

10. M.S. Venkatraman, I.S. Cole, B. Emmanuel, *Electrochim . Acta*, 56 (2011) 8192 .

11. J.D. Yoo, K. Ogle, P. Volovitch, *Corros. Sci*. 83 (2014) 32.

12. D.D. Macdonald, *Pure Appl. Chem*. 71 (6) (1999) 951.

13. D.D. Macdonald, K.M. Ismail, E. Sikora, *J. Electrochem. Soc*. 145 (1998) 3141.

14. C.a. Laska, M. Auinger, P. Biedermann, D. Iqbal, N. Laska, J. De Strycker, K.J. Mayrhofer, *Electrochim. Acta* 159 (2015) 198.

15. M. Prestat, L. Holzer, B. Lescop, S. Rioual, C. Zaubitzer, E. Diler, D. Thierry, *Electrochem.Commun.* 81,(2017) 56.

16. C. Cachet, C.P. De Pauli, R. Wiart, *Corros. Sci*. 25 (1985) 493.

17. S. Walkner, A.W. Hassel, *Electrochim. Acta* (2014) 130.

18. S. Thomas, I. Cole, M. Sridhar, N. Birbilis, *Electrochim. Acta* 97 (2013) 192.

19. L. M. Baugh, A. Higginson, *Electrochim. Acta* 30 (1985) 1163.

20. S. Thomas, N. Birbilis, M.S. Venkatraman, I.S. Cole, *Corrosion* 68 (2012) C015009-1.

21. X.G. Zhang, *Corrosion and Electrochemistry of Zinc*, plenum pre Edition, New York, 1996.

22. Z. Pilbáth, L. Sziráki, *Electrochim. Acta* 53 (2008) 3218.

23. S. Bonk, M. Wicinski, A.W. Hassel, M. Stratmann, *Electrochem. Commun*. 6 (2004) 800.

24. I. Odnevall Wallinder, C. Leygraf, *Reaction sequences in atmospheric corrosion of zinc, in: W. Kirk, H. Lawson (Eds.), Atmospheric Corrosion, ASTM STP 1239, Philadelphia, 1995, p. 215.*

25. S. Thomas, N. Birbilis, M. Venkatraman, I. Cole, *Corros. Sci*. 69 (2013) 11,

26. R. armaitis, V. Dikinis, and V. Rezaite *Protection of Metals, Vol. 39, No. 4, 316.(2003)*

27. P. LI. Cabot, M. Cortes, F. A. Centellas, J. A. Garrido and E. Wra, *J. Elecroanal. Chem*. 201, 85 (1986).

28. L. Kaili, H. Ping, B. Hongmei , C. Jingchao , D. Faqin , W. Shengbing , H. Mingqian , Y. Shengping, *Mater. Chem. Phys*.199 (2017) 73.

29. S. Thomas, I.S. Cole, M. Sridhar, N. Birbilis *Electrochim. Acta* 97, (2013)192.

30. L. Sziraki, E. Szocs, Zs. Pilbath, K. Papp, E. Kalman *Electrochim Acta* 46 (2001) 3743

31. G.A.G. Pedroza, C.A.C.de Souza, I.A. Carlos, L.R.P. de Andra Lima, *Surf.Coat.Tech*. 206, (2012) 2927

32. Mohamed A. Amin, Hamdy H. Hassan, Sayed S. Abd El Rehim. *Electrochim. Acta*. 53, (2008)2600.

33. A.K. Neufeld, I.S. Cole, A. Bond, S. Furman, *Corr. Sci*. 44 (2000) 555.

34. Tim H. Muster, Ivan S. Cole, *Corros. Sci*. 46, (2004)2319.

35. *Powder Diffraction file, Joint Commitee ON Powder Diffraction Standard, A.S.T.M. Philadelphia, PA, 1967, Card 369-1451 (Zincite).*

36. M. Izaki, T. Omi, *J. Electrochem. Soc*. 143 , (1996) L.53.

37. A. Goux, T. Pauporte , J. Chivot, D. Lincot, *Electrochim. Acta* 50, (2005) 2239

38. D. Calestani, M. Zha , R. Mosca , A. Zappettini , M.C. Carotta , V. Di Natale , L. Zanotti *Sens. Actuator B. Chem*.144, (2010) 472.

39. Magdalena Skompska, Kamila Zarebska ¸ *Electrochim. Acta,* 127, (2014) 467.

40. H.Q. Bian, S.Y. Ma n, Z.M. Zhang, J.M. Gao, H.B. Zhu, *J. Cryst. Growth*, 394, (2014) 132.

41. Noha Samir, Dina S. Eissa, Nageh K. Allam , *Mater. Lett*.137 (2014) 45.

42. Aurangzeb Khan, Wojciech M. Jadwisienczak, Martin E. Kordesch, *Physica E33*, (2006) 331.
43. U. O zgur, Y. Alivov, C. Liu, A. Teke, M. Reshchikov, S. Dog-brevean, V. Avrutin, S.J. Cho, H. Morkoc, *J. Appl. Phys.* 98, (2005) 041301.
44. J.Q. Hu, X.L. Ma, Z.Y. Xie, N.B. Wong, C.S. Lee, S.T. Lee, *Chem. Phys. Lett.* 344(2001) 97.
45. S. Mahamuni, K. Borgohain, B.S. Bendre, V.J. Leppert, S.H. Risbud, *J. Appl. Phys*. 85, (1999)2861.
46. Li Su, Ni Qin *Ceram. Inter*. 41, 2673 (2015).